RSC Advances

ROYAL SOCIETY OF CHEMISTRY

www.rsc.org/advances

Journal Name

ARTICLE

Switching Mechanism of Al/$La_{1-x}Sr_xMnO_3$ Resistance Random Access Memory. I. Oxygen Vacancy Formation in Perovskites

Received 00th January 20xx,
Accepted 00th January 20xx

DOI: 10.1039/x0xx00000x

www.rsc.org/

Nodo Lee,[a†] Yves Lansac,[b] Hyunsang Hwang,[c] and Yun Hee Jang[a*]

Resistance random access memory is a promising next-generation non-volatile memory device due to its simple capacitor-like structure, ultrafast switching, and extended retention. A composite thin film of perovskite oxide such as $La_{1-x}Sr_xMnO_3$ (LSMO) and reactive metal such as aluminum (Al) is a key material for such device, but lack of clear understanding of its microscopic switching mechanism hampers further development along this direction. We therefore carry out a series of density functional theory calculations tracking down a molecular-level hypothesis of the switching process: (1) oxygen vacancy (V_O) formation in LSMO and migration through LSMO towards the interface with Al and (2) AlO_x oxide formation at the interface. As the first step of this series of effort, Al/LSMO/Al model junction devices are built to represent four different oxygen-deficiency levels of LSMO, and their structure, energy, electronic structure, and current-voltage characteristics are calculated and compared. We find that the V_O formation in LSMO itself plays an interesting role in the resistive switching of the junction by initially reducing the number of majority-spin states around the Fermi level (becoming more insulating as expected) and then by increasing the number of minority-spin states through Mn-V_O-Mn-V_O filament-like pathways developed in the film (surprisingly becoming more conducting than stoichiometric LSMO). Assessment of the importance of this effect would require a comparison with the ON/OFF ratio induced by AlO_x formation, which will be done separately in the second step of our effort, but the control of the oxygen deficiency appears to be a very important and challenging task required for reliable device fabrication and operation. The calculation also shows that, at sufficiently high doping level x, the V_O formation energy is reasonably low and the V_O migration energy barrier is even lower, explaining the fast switching of this type of devices. On the other hand, the calculated energy barrier is high enough to avoid thermal random-walk O migration which could refill V_O sites, explaining the extended retention of such devices.

Introduction

Across nanoscale thin films, even a low applied voltage corresponds to a large electric field that can cause charged species to move.[1,2] A resistive switching coupled with the voltage-induced movement of charged species occurring in a metal-oxide-metal capacitor-like thin film [so-called electric-pulse-induced resistance change,[3-7] colossal electroresistance[8,9] or redox-based electrochemical nanoionics[2,10,11]] forms the basis of resistance (switching) random access memory (RRAM).[12,13] Due to its simplicity, ultrafast read/write/erase, low operation voltage, and extended retention of each bi-stable (or possibly multi-stable) resistive state,[14] RRAM has a great potential as a next-generation high-density non-volatile memory.[12,13,15,16]

Such resistive switching is classified into two types, unipolar and bipolar, depending on the polarity of the write/erase (ON/OFF) voltages.[1,2,12,13,17] Current-induced thermophysical (due to the Joule heating)[10,17] formation-rupture of nm-scale conductive filaments in an insulating oxide matrix is considered responsible for unipolar (symmetric) switching observed in MIM-type thin-film devices (I = NiO, TiO_2; M = Pt).[13,18-23] A bipolar (antisymmetric) resistive switching, which requires both polarities of voltages (one to set to an ON state and the reverse to reset to an OFF state), is observed in similar MIM'-type heterojunction devices (I = ZnO, SiO_2, Al_2O_5, ZrO_2, Ta_2O_5, TiO_2; M = Pt, W; M' = Ag, Cu) via so-called electrochemical metallization (or conductive bridging).[10,11,24-27]

Another type of bipolar switching is exhibited by heterojunction devices composed of insulating or semiconducting perovskite oxide [$Pr_{1-x}Ca_xMnO_3$ (PCMO), $La_{1-x}Ca_xMnO_3$ (LCMO), $La_{1-x}Sr_xMnO_3$ (LSMO), $La_{1-x}Ba_xMnO_3$ (LBMO)] attached to reactive metal (Al, Sm, Ti).[3-8,28-45] Microscopic mechanism of this phenomenon is still unclear,[2,12,13,46] except that the high-resistance state comes from a facile formation of an interfacial metal oxide layer (AlO_x, SmO_x, TiO_x) after a reaction of the reactive metal with the oxygen ions migrated from the perovskite oxide and that such layer-type (rather than filament-type) transition greatly improves the switching ratio and the die-to-die uniformity[47] so that even a possibility of a multi-level operation is demonstrated using LSMO.[40] Therefore most studies of the resistive switching mechanism[27,48-53] have focused on the role played by the reactive metal and its oxides without paying much attention to the role played by the perovskite.

However, LSMO and other perovskite manganites[54] are in fact the most studied materials for colossal magnetoresistance[55,56] and

[a] School of Materials Science and Engineering, Gwangju Institute of Science and Technology, Gwangju 61005, Korea
[b] GREMAN, UMR 7347, Université François Rabelais, 37200 Tours, France
[c] Department of Materials Science and Engineering, Pohang University of Science and Technology, Pohang, 790-784, Korea
† Present address: LG Electronics Advanced Research Institute, Seoul, Korea
* Corresponding author: Yun Hee Jang (yhjang@gist.ac.kr)

they are known to exhibit sharp metal-to-insulator transitions upon oxygen deficiency:[57-61] they exhibit both colossal magnetoresistance and colossal electroresistance.[40] We therefore speculate that the sensitive oxygen-vacancy-induced variation of resistivity in bulk LSMO perovskites could also be (a part of) the origin of the bipolar resistive switching of their junctions with reactive metals (Al/LSMO, for example). Indeed, oxygen vacancies already created in LSMO in the course of device fabrication, whose contents are controlled with reactive metals, are known to improve the ON/OFF ratio.[42] Understanding the oxygen-defect chemistry of perovskites (LSMO) separately from the oxide-formation chemistry of reactive metals (Al) should be crucial for understanding the resistive switching mechanism and designing high-performance RRAM materials from a combinatorial approach. However, these two effects are so entangled that it should be extremely difficult to separate them out in real-world experiments.

Therefore in this work we perform a virtual experiment where density functional theory (DFT) calculations are carried out to study the oxygen-vacancy-induced resistivity change in Al/LSMO/Al model junctions without the intervention of concurrent AlO_x formation at the interface, which will be studied separately and combined with this work later. Energetics of the oxygen vacancy formation and migration in bulk LSMO as well as the electronic structure of the oxygen-deficient LSMO are also studied. This is an extension of our previous studies where DFT calculations were carried out first on the smallest Al/LSMO/Al junction models made of an ideal cubic structure of LSMO[62] and then rather seriously on the orthorhombic structure of stoichiometric bulk LSMO.[63] We now introduce various concentrations of oxygen vacancies in the orthorhombic structure of parents and mixed-valence LSMO ($La_{1-x}Sr_xMnO_{3-\delta}$ with x = 0, 0.25, 0.5, and 1 and δ = 0, 0.17, 0.25, 0.33, 0.5, 0.67, and 1).

Computational Details

A spin-polarized DFT calculation with the Perdew-Burke-Ernzerhof (PBE) exchange-correlation functional[64,65] is carried out using VASP (Vienna ab initio simulation package).[66,67] The PBE functional is known to quite well reproduce the structure, electronic structure, and magnetic properties of manganites.[68-71] Projector-augmented-wave pseudopotentials replace the core electrons of each atom,[67,72] and the valence electrons [11 in La 5*s*/5*p*/6*s*/5*d*, 10 in Sr 4*s*/4*p*/5*s*, 7 in Mn 4*s*/3*d*, and 6 in O 2*s*/2*p*] are described by a set of plane waves with kinetic energies up to 550 eV. The convergence criterion is 10^{-5} eV for electronic self-consistent-field (SCF) cycles and 10^{-4} eV for conjugate-gradient ionic update cycles. The Monkhorst-Pack k-point mesh[73] is used to sample the Brillouin zone with the size of (6×6×6) for β-$SrMnO_3$, (6×5×6) for $LaMO_3$ and $La_{1-x}Sr_xMO_3$ (x = 0.25 and 0.5), and (6×3×4) for α-$SrMnO_3$ for geometry optimization (See the size of the unit cells below in Table 1). All the structures are built and visualized with VESTA.[74] For further electronic structure analyses at each optimized geometry, a single-point-energy PBE+U calculation is carried out with a carefully-chosen U parameter (2.0 eV), despite a debate on the choice of U.[75-81] Density of states (DOS) is visualized with a Gaussian smearing with a width of 0.1 eV. Atomic charges and magnetic moments are obtained with the Bader analysis.[82-84] The transmission spectra and the *I-V* curves of Al/LSMO/Al model junction devices are calculated with the non-equilibrium Green's-function (NEGF) formalism implemented in ATK (Atomistix Tool Kit).[86,87] The Trouillier-Martins norm-conserving nonlocal pseudopotentials[88] replace the core electrons and a single-zeta-polarization Gaussian-type localized basis set describes the valence electrons. A (60×60) k-point sampling is used.

Results and discussion

Stoichiometric $La_{1-x}Sr_xMnO_3$ (*x* = 0, 0.25, 0.5, and 1)

Parent $LaMnO_3$ (LMO; x = 0) is rhombohedral and monoclinic above 970 K,[89] cubic (with dynamic fluctuation) above 750 K,[90-92] and orthorhombic at room and low temperatures.[90,93-96] $SrMnO_3$ (SMO; x = 1) is hexagonal (α-SMO) and becomes orthorhombic around 100 K,[97-100] but both share essentially the same primitive-cell structure. SMO can be also cubic (β-SMO) at room temperature[85,97,101,102] but only after annealing α-SMO from ~1673 K.[85,103] A significant oxygen-deficiency is expected at such high temperature ($SrMnO_{3-\delta}$) and oxidation during annealing is required to restore the stoichiometric β-SMO,[85,97,101,102] implying that cubic β-SMO should be an oxygen-deficient non-stoichiometric phase.

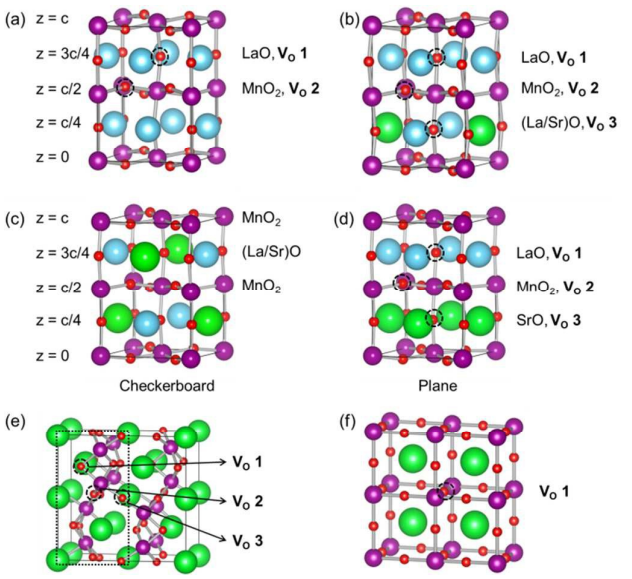

Fig. 1. LSMO unit cells and unique V_O sites. (a) x = 0 (orthorhombic LMO; 4 f.u.) with two unique V_O sites, (b) x = 0.25 with three, (c-d) x = 0.5 with checkerboard- and plane-type La/Sr ordering where the latter has three, and (e-f) x=1 (orthorhombic α-SMO with three and 2×2 supercell of cubic β-SMO with only one). Color code: La (blue), Sr (green), Mn (purple), O (red), and V_O site (black circle).

Table 1. Crystal structures of parent manganites (LMO and SMO).

		a	b	c	ρ	∠(MnOMn)
LMO	Exp[a]	5.74	7.70	5.54	6.57	155.5±1.1
AFM-A	Calc	5.66	7.77	5.57	6.56	155.3±1.0
	Error	1.5%	1%	0.6%	0.13%	0.1%
α-SMO	Exp[a]	5.44	9.42	9.06	5.45	175.8±1.3
AFM-A	Calc.	5.50	9.51	9.14	5.30	170.6±2.0
	Error	1%	0.9%	0.8%	2.7%	2.9%
β-SMO	Exp[a]	3.80	-	-	5.75	180
AFM-G	Calc	3.83	-	-	5.63	180
	Error	0.7%	-	-	2.1%	0%

[a] Refs. 85,93,100; lattice constant (a-c) in Å; density (ρ) in g/cm^3; angle (∠) in °.

The crystal structures of orthorhombic LMO, orthorhombic α-SMO, and cubic β-SMO, which consist of four, eight, and one formula units (f.u.) per unit cell, are selected and fully optimized (Fig. 1). Indeed, orthorhombic α-SMO is calculated more stable (by 0.3 eV/f.u.) than cubic β-SMO. The magnetic ground state is also predicted: FM (ferromagnetic) and A-type AFM (antiferromagnetic) for LMO and A-type and G-type AFM for SMO, which agree with experiments.[56,85,93,99,100,104,105] The lattice constants and the internal structural parameters (Mn-O-Mn angle) optimized at their magnetic ground states are within 3% from the experiments (Table 1),[85,93,100] correctly reflecting the greater Jahn-Teller distortion in LMO (155°) than in SMO (~180°).[85,90,93-96,100,101] The magnetic moment (in μ_B) calculated for Mn in orthorhombic FM LMO (3.81) well reproduces experiment (3.81)[93] and hybrid-functional (Heyd-Scuseria-Ernzerhof; HSE)[106,107] DFT calculations (3.84).[79] All these results indicate the reliability of our method employed in the following calculations.

Mixed-valence LSMO crystals can be tetragonal, orthorhombic, rhombohedral, or monoclinic, depending on doping level x, oxygen deficiency δ, and synthesis conditions.[56,85,108] LSMO at doping levels of 0.25-0.3 and 0.5 lie near the rhombohedral-orthorhombic[56,109,110] and tetragonal-orthorhombic[85,111] phase boundaries, respectively, at low temperatures. In fact their lattice constants are similar within 2% and their total energies are calculated similar within 8 meV. We thus use the orthorhombic phase of LMO (*Pnma* with 4 f.u.)[93] to build the orthorhombic mixed-valence LSMO (x = 0.25 and 0.5) by replacing a given amount (x) of La with Sr. We consider only FM magnetic ordering, based on experimental reports on FM ordering of LSMO (x > 0.15).[56,112] Among two types (checkerboard or plane) of A-site (La/Si) ordering in LSMO (x = 0.5; Figs. 2c-d), we consider only the plane type,[77,113-115] which is calculated to be more stable (by 0.12 eV) than the checkerboard type. The average Mn magnetic moment (in μ_B) decreases with increasing the Sr concentration x [3.81 (0); 3.61 (0.25); 3.39 (0.5)] consistently with the experimental trend [3.81 (0); 3.48 (0.3); 3.38 (0.4)].[93,116] This should be because Sr^{2+} replacement of La^{3+} would induce Mn^{4+} ($4d^3$) replacement of Mn^{3+} ($4d^4$) for the charge valence. The DOS (black) and PDOS (color) curves in Figs. 2a-b show that stoichiometric mixed-valence LSMO (x = 0.25 and 0.5) keeps the typical half-metallic behaviour of parent LMO and that the majority (up) and minority (down) spin states near the Fermi level (E_F) mainly come from Mn (purple) and O (red). The contribution of La and Sr (not shown) to these states near E_F is negligible. We also notice a slight shift of the DOS curves towards a lower binding energy (to the right side in Fig. 2) with increasing the Sr doping level x, which is considered as a hole-doping effect.[117] All these are consistent with the findings from the HSE calculation.[79]

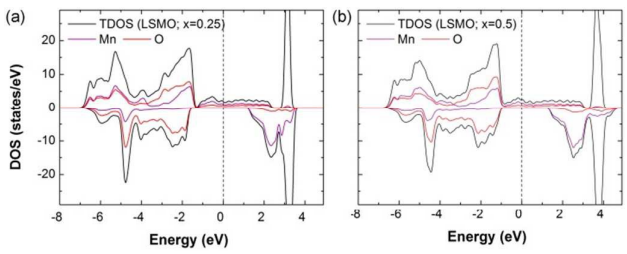

Fig. 2. Spin-polarized (majority/minority spins in upper/lower regions) DOS (black) and PDOS (colored) curves (relative to E_F set to zero) of orthorhombic LSMO (x = 0.25, 0.5).

Formation of a single oxygen vacancy in LSMO (x = 0 to 1)

A single oxygen vacancy (V_O; conc. 8.3%) is created and relaxed at different sites in the optimized unit cells of LSMO (black circle; Fig. 1). The V_O formation energy (E_{VO}), that is, the energy cost to form a V_O is defined as:

$$E_{VO} = E(La_{1-x}Sr_xMnO_{3-\delta}) + \tfrac{1}{2}E(O_2) - E(La_{1-x}Sr_xMnO_3), \qquad (1)$$

where $E(La_{1-x}Sr_xMnO_{3-\delta})$ or $E(LSMO_{3-\delta})$, $E(La_{1-x}Sr_xMnO_3)$ or E(LSMO), and $E(O_2)$ are the energy of bulk LSMO with and without V_O (Fig. 1) and the energy of a triplet O_2 in the gas phase (modelled by an empty cubic unit cell of 15 Å). The calculated E_{VO} values (in eV) are: 4.22 and 4.39 from LaO (V_{O1}) and MnO_2 (V_{O2}) planes of LMO (x = 0; Fig. 1a); 4.01, 3.98, and 4.17 from LaO (V_{O1}), MnO_2 (V_{O2}), and LaSrO (V_{O3}) planes of LSMO (x = 0.25; Fig. 1b); 3.39 (V_{O1}), 3.44 (V_{O2}), and 3.69 (V_{O3}) from LSMO (x = 0.5; Fig. 1d); 1.92 from a (2x2) super cell of cubic β-SMO (x = 1; Fig. 1f). Our E_{VO} values for LMO (4.22-4.39) are close to literature values: 4.16 calculated for cubic LMO (V_O conc. 4.2%)[118] and 4.29 from a cluster-defect model,[119] although a higher value (4.85) has also been reported.[120] The most striking feature revealed by our calculation (Fig. 3a) is that the average E_{VO} decreases almost linearly with the doping level x in agreement with an experimental finding.[119] This is understandable because LSMO with La^{3+} replaced by Sr^{2+} would tend to maintain its charge neutrality by turning Mn^{3+} into Mn^{4+} (as seen in the previous section) or by losing O^{2-} (as seen here). Our E_{VO} values for LSMO with 0.25-0.5 of x (~4 eV) are comparable to the typical operation voltages (4-4.5 V).[33,36] Highly-doped LSMO (only up to x ≈ 0.5 due to a stability issue) could easily create V_O (most likely during device fabrication), improving the RRAM ON/OFF ratio,[42] the threshold voltage for device operation, and the operation speed.

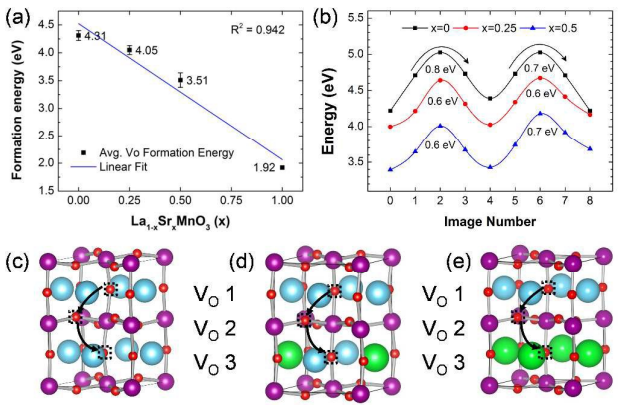

Fig. 3. (a) Average V_O formation energy in LSMO; (b) Energy profile for V_O migration into adjacent V_O sites (dotted square) along the minim-energy pathways (black arrows) in orthorhombic LSMO with x = 0 (c), 0.25 (d), and 0.5 (e).

Migration of a single V_O in LSMO (x = 0, 1/4, and 1/2)

A facile V_O formation in LSMO should be related with a facile oxygen transport through LSMO under bias voltages. We therefore search for the minimum-energy oxygen-migration (V_O-migration) pathways in LSMO (x = 0, 0.25, and 0.5; Figs. 3c-e) and calculate the energy changes along the pathways, using the climbing image nudged elastic band method[121,122] implemented in VASP. These oxygen migration energy profiles combined with the E_{VO} values calculated

in the previous section [4.3 (x = 0; black), 4.0 (x = 0.25; blue), and 3.5 (x = 0.5; red) eV at the image number 0] are shown in Fig. 3b. Surprisingly, the activation barrier of oxygen migration is calculated as 0.6-0.8 eV for all three LSMO's irrespective of the doping level x, contrary to E_{VO} which significantly decreases with x (4.3 to 3.5 eV). The oxygen migration in bulk L(S)MO has been extensively studied for high-temperature (~1000 K) solid-oxide fuel-cell applications: Low diffusion barriers estimated from molecular dynamics simulations (<1 eV)[123-126] and from electrochemical measurements (0.73 eV for x = 0.2)[127] agree well with our estimates (0.6-0.8 eV). Comparable diffusion barriers (0.4 and recently 0.9±0.2 eV) have been estimated in Pt/PCMO/Pt (x ≈ 0.3) devices.[7,35] In all the cases the V_O migration barriers stay much lower than E_{VO}, implying that, once V_O is created, the switching speed may not depend critically on the doping level x. Such low migration barriers may explain the fast switching of perovskite-based RRAM devices. On the other hand, since the migration barriers are sufficiently high to block thermal random-walk V_O migrations at room temperature, the V_O sites would not be refilled randomly without voltage applied, explaining the extended retention of this type of RRAM devices.

Electronic structure of oxygen-deficient LSMO (x = 1/4 and 1/2)

The average Mn magnetic moment (in μ_B), which decreased from 3.81 of parent LMO (x = 0) to 3.61 (x = 0.25) and to 3.39 (x = 0.5) of mixed-valence LSMO, increases back to 3.91 (x = 0.25) and 3.73 (x = 0.5) when a single V_O (conc. 8.3%) is introduced and stays around 3.80 (x = 0.25) and 3.73 (x = 0.5) when the second V_O is created (conc. 16.7%) to form the most stable double-V_O configuration (Mn-V_O-Mn-V_O perpendicular to LaO/SrO planes). It is understandable because mixed-valence LSMO with La^{3+} replaced by Sr^{2+}, which maintained its charge neutrality by turning Mn^{3+} (d^4) into Mn^{4+} (d^3) lowering the magnetic moment, now puts back Mn^{3+} (increasing the magnetic moment) to fix charge imbalance caused by lost O^{2-} Ions.

The DOS curves of LSMO (x = 0.5, Fig. 4; essentially the same curves are obtained for x = 0.25, not shown) show that non-stoichiometric LSMO with a single V_O (V_O conc. 8.3%; Fig. 4a) still keeps the typical half-metallic characteristic of stoichiometric LSMO irrespective of the position of the V_O site (V_{O1}, V_{O2}, or V_{O3}). Only defect states appear near the bottom of the conduction band of the minority spin (at ~1 eV) and reduces the minority-spin gap to 2.49 (x = 0.25) and 1.99 (x = 0.5) eV. This is comparable to the study of Wang and coworkers, which has shown the reduced half-metallic gap of rhombohedral LSMO with V_O conc. up to 8.3%.[69]

On the other hand, the half-metallic characteristic of LSMO disappears when the second V_O is introduced to form Mn-V_O-Mn-V_O paths (V_O conc. 16.7%; Fig. 4b). The majority spin density decreases around E_F by ~50%, while the minority spin density slightly increases. Since the conductivity is in general proportional to the number of states at E_F, the oxygen loss from the Mn-O-Mn-O paths would result in a significant reduction of the majority-spin conductivity of LSMO,[128] but an increase in the minority-spin conduction is also expected. It is not therefore clear yet how (more specifically, in which direction, positive or negative) the V_O formation in LSMO would contribute to the resistive switching of Al/LSMO-based RRAM devices. We need to quantify the contribution of the V_O formation in LSMO to electron transport (current, conductivity, or resistivity).

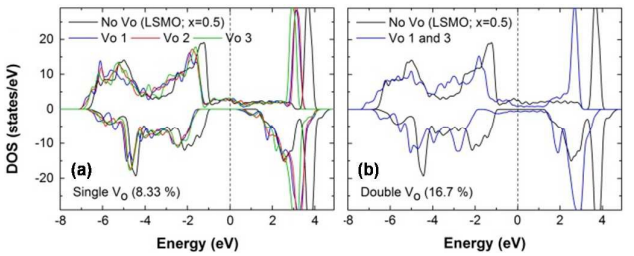

Fig. 4. Spin-polarized DOS of LSMO (x = 0.5) at V_O conc. 8.3% and 16.7%. LSMO (x = 0.25) shows essentially the same behaviour (not shown here).

Electron transport through oxygen-deficient LSMO (x = 1/3)

We therefore quantify the contribution of the V_O formation in LSMO to the resistive switching of Al/LSMO devices. This is done by comparing electron transport (transmission and *I-V* curves) of the Al/LSMO/Al model devices calculated at different V_O conc. in LSMO (x = 0.5). To build a model device at each V_O concentration, the lowest-energy V_O configuration of LSMO (x = 0.5 with a plane-type La/Sr ordering) is selected, cut into a seven-atomic-layer symmetric LSMO(001) thin film with the MnO_2 termination[129] (MnO_2-LaO-MnO_2-SrO-MnO_2-LaO-MnO_2), redefined as a (√2×√2)R45° unit cell and attached to a (2×2) supercell of three-atomic-layer Al(001) film at each side in order to minimize the junction mismatch (3.5%). The atomic positions of LSMO and two adjacent Al layers at each side are relaxed with the outermost Al layer at each side fixed at its bulk position and lattice parameter (8.05 Å). This optimized scattering region (Figs. 5b-e) is attached to a (2×2) supercell of additional thirteen Al(001) layers at each side (Fig. 5a) to avoid a failure in SCF convergence of the NEGF calculations. Our choice of symmetric junction models (LaO-SrO-LaO) would give the conductivity of LSMO (x = 0.33) instead of LSMO (x = 0.5). In all the cases, this doping level (x = 0.33) corresponds to the most interesting doping level for device applications[3-7] [due to the highest Curie temperature (380 K) at x ≈ 0.3.[55,56]] A layered configuration of $2V_O$ and $4V_O$ (conc. 5.7% and 11%; Figs. 5c-d) with all the V_O's from the same LaO plane, which is at least 0.22 eV more stable than other configurations, is chosen. Since these layered V_O's are significantly more stable in LaO or SrO planes than in MnO_2 planes, a layered configuration of $12V_O$ made by removing all the O's from La(Sr)O planes (conv. 33%; Fig. 5e) to form a full amount of Mn-V_O-Mn-V_O paths is also considered.

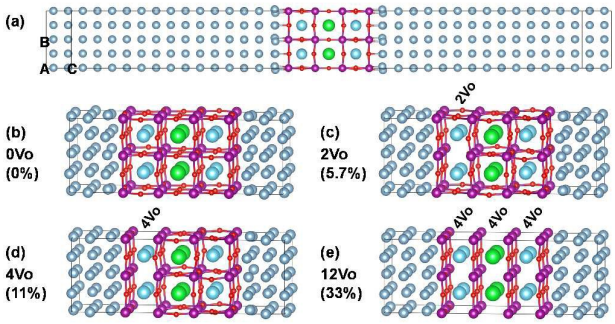

Fig. 5. Al/LSMO/Al model devices at different V_O concentrations (0, 5.7, 11, and 33%).

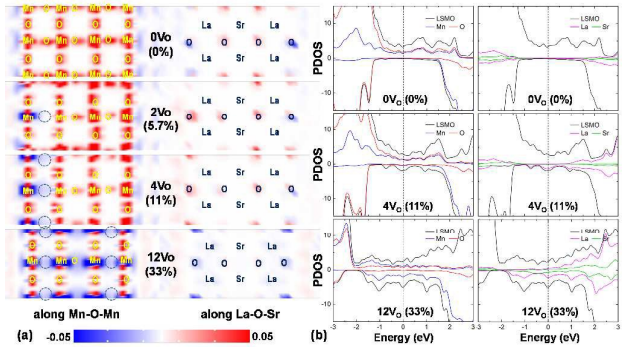

Fig. 6. (a) Spin-resolved (blue/red) LDOS ($Å^{-3}eV^{-1}$) projected onto LSMO(100) planes cut along Mn-O-Mn (left) and La-O-Sr (right) chains perpendicular to the junction interfaces and (b) PDOS projected onto La, Sr (right), Mn, and O (left) of LSMO at different V_O concentrations.

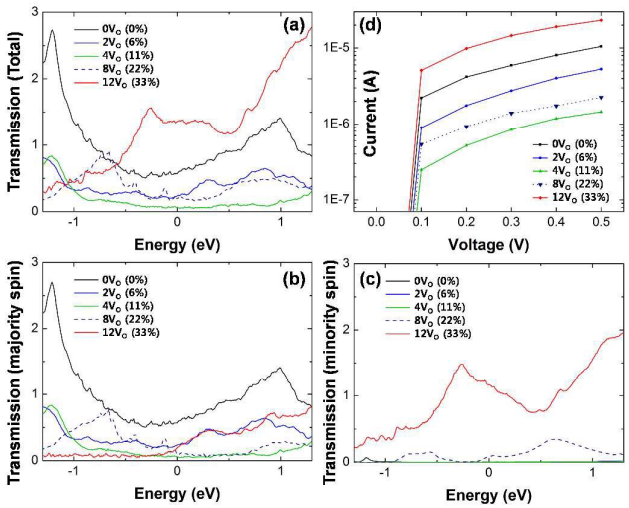

Fig. 7. (a-c) Total and spin-polarized (majority-spin and minority-spin) transmission and (d) *I-V* curves of Al/LSMO/Al at different V_O concentrations.

The spatially-resolved local DOS (LDOS) on the LSMO(100) planes cut along the Mn-O-Mn and La-O-Sr chains perpendicular to the Al/LSMO/Al junction interfaces (Fig. 6a) as well as the PDOS of La, Sr, Mn, and O in the Al/LSMO/Al junctions (Fig. 6b) show the same spin-polarized characteristics found in bulk LSMO in the previous sections. Up to $4V_O$ (conc. 11%) where all the V_O's are confined in a single LaO plane, the half-metallic behaviour of the schoichiometric LSMO is still maintained and the major contribution around E_F comes from the majority-spin states of Mn and O. Hence the transmission (Figs. 7a-c) is allowed only for the majority spins. There is no transmission of minority spins due to the minority-spin gap larger than 2 eV near E_F. This majority-spin transmission near E_F steadily decreases with increasing V_O concentration up to 11% ($4V_O$) where it is completely eliminated while minority-spin transmission is still negligible, resulting in an order-of-magnitude reduction of the current (Fig. 7d, black to green). This could be related with the typical ON/OFF ratio of ~10 observed for the junctions between PCMO and inert layers such as Pt.[3,33] It is surprising to see such a drastic change in the transmission since the major-spin PDOS changes so little in this range of V_O concentration (Fig. 6b). Fig. 6a indicates that V_O formation induces spin-flipping of Mn atoms next to V_O. A single spin-flipped Mn atom per Mn-O-Mn-O conduction path at V_O conc. 11%, which corresponds to a negligible amount in DOS, appears to be sufficient to cut the conduction path and switch OFF the transmission.

On the other hand, at the high V_O conc. of 33% ($12V_O$) where Mn-V_O-Mn-V_O filament-like pathways form across the thin film of LSMO, a significant amount of minority-spin states develop near E_F due to spin-flipped Mn atoms next to V_O's (Fig. 6b). This series of spin-flipped Mn atoms along Mn-V_O-Mn-V_O chains are now close enough to overlap with each other (Fig. 6a) and form filament-like major transmission channels (Fig. 7c), dramatically increasing the total transmission and the current (Figs. 7a-b, green to red). Surprisingly LSMO at this V_O concentration is even more conductive (ON) than stoichiometric LSMO, cancelling out the OFF state of the coexistent AlO_x layer and reducing the ON/OFF ratio of the device.

These results suggest that (1) the electron transport of Al/LSMO-based RRAM devices is sensitive to the V_O concentration in LSMO; (2) the intrinsic contribution from the V_O formation in LSMO to the resistive switching of the device would be the ON/OFF current ratio of 10^1 at most (which could be smaller than the contribution from the AlO_x formation, as will be reported separately); and (3) overly high V_O concentration in overly thin LSMO films may form filament-like additional minority-spin conduction channels and end up with a reduction of the ON/OFF ratio by ~10^1 unless only the majority-spin current is detected.

Conclusions

Carefully-validated DFT and NEGF calculations on oxygen-deficient LSMO show that (1) the first step for the resistive switching of Al/LSMO-based RRAM, V_O formation-migration, could be realized with reasonable energy (for reasonable operation voltage, speed, and retention) in highly-doped LSMO in particular; (2) the ON/OFF ratio of the V_O-induced resistive switching of LSMO would increase only up to the point where minority-spin current channels along filament-like Mn-V_O-Mn-V_O chains start to cut across the whole thin layer of LSMO; and (3) this contribution from V_O formation in LSMO to the total ON/OFF ratio of Al/LSMO-based RRAM could be smaller than the contribution from concurrent AlO_x formation, as will be reported separately.

Acknowledgements

This work was supported by the Global Frontier Hybrid Interface Materials (2013M3A6B1078882), CCS 2020 (2014M1A8A1049267 & 2014M1A8A1049321), and Basic Research (2013R1A1A3012254) Programs of the Korean National Research Foundation, the Brain Pool Program (151S-1-3-1232) of KOFST, the DGIST-GIST Project of DGIST, the Specialized Research Project of GIST, and the PLSI and Grand Challenge (KSC-2015-C3-014) Programs of KISTI.

Notes and references

1 D. B. Strukov, G. S. Snider, D. R. Stewart and R. S. Williams, *Nature*, 2008, **453**, 80.
2 R. Waser and M. Aono, *Nat. Mater.*, 2007, **6**, 833.

3 S. Q. Liu, N. J. Wu and A. Ignatiev, *Appl. Phys. Lett.*, 2000, **76**, 2749.
4 A. Baikalov, Y. Q. Wang, B. Shen, B. Lorenz, S. Tsui, Y. Y. Sun, Y. Y. Xue and C. W. Chu, *Appl. Phys. Lett.*, 2003, **83**, 957.
5 X. Chen, N. J. Wu, J. Strozier and A. Ignatiev, *Appl. Phys. Lett.*, 2005, **87**, 233506.
6 X. Chen, N. Wu, J. Strozier and A. Ignatiev, *Appl. Phys. Lett.*, 2006, **89**, 063507.
7 Y. B. Nian, J. Strozier, N. J. Wu, X. Chen and A. Ignatiev, *Phys. Rev. Lett.*, 2007, **98**, 146403.
8 A. Sawa, T. Fujii, M. Kawasaki and Y. Tokura, *Appl. Phys. Lett.*, 2004, **85**, 4073.
9 A. Sawa, T. Fujii, M. Kawasaki and Y. Tokura, *Appl. Phys. Lett.*, 2006, **88**, 232112.
10 I. Valov, R. Waser, J. R. Jameson and M. N. Kozicki, *Nanotechnology*, 2011, **22**, 254003.
11 I. Valov, E. Linn, S. Tappertzhofen, S. Schmelzer, J. van den Hurk, F. Lentz and R. Waser, *Nat. Commun.*, 2013, **4**, 1771.
12 A. Sawa, *Mater. Today*, 2008, **11**, 28.
13 R. Waser, R. Dittmann, G. Staikov and K. Szot, *Adv. Mater.*, 2009, **21**, 2632.
14 A. Beck, J. G. Bednorz, C. Gerber, C. Rossel and D. Widmer, *Appl. Phys. Lett.*, 2000, **77**, 139.
15 A. Kingon, *Nat. Mater.*, 2006, **5**, 251.
16 K. Szot, W. Speier, G. Bihlmayer and R. Waser, *Nat. Mater.*, 2006, **5**, 312.
17 F. Pan, C. Chen, Z.-s. Wang, Y.-c. Yang, J. Yang and F. Zeng, *Prog. Nat. Sci.: Mater. Int.*, 2010, **20**, 1.
18 S. Seo, M. J. Lee, D. H. Seo, E. J. Jeoung, D. S. Suh, Y. S. Joung, I. K. Yoo, I. R. Hwang, S. H. Kim, I. S. Byun, J. S. Kim, J. S. Choi and B. H. Park, *Appl. Phys. Lett.*, 2004, **85**, 5655.
19 D. C. Kim, S. Seo, S. E. Ahn, D. S. Suh, M. J. Lee, B. H. Park, I. K. Yoo, I. G. Baek, H. J. Kim, E. K. Yim, J. E. Lee, S. O. Park, H. S. Kim, U. I. Chung, J. T. Moon and B. I. Ryu, *Appl. Phys. Lett.*, 2006, **88**, 202102.
20 J. J. Yang, M. D. Pickett, X. Li, D. A. A. Ohlberg, D. R. Stewart and R. S. Williams, *Nat. Nanotechnol.*, 2008, **3**, 429.
21 D. H. Kwon, K. M. Kim, J. H. Jang, J. M. Jeon, M. H. Lee, G. H. Kim, X. S. Li, G. S. Park, B. Lee, S. Han, M. Kim and C. S. Hwang, *Nat. Nanotechnol.*, 2010, **5**, 148.
22 K. M. Kim, B. J. Choi, M. H. Lee, G. H. Kim, S. J. Song, J. Y. Seok, J. H. Yoon, S. Han and C. S. Hwang, *Nanotechnology*, 2011, **22**, 254010.
23 D. Lee, J. Park, J. Park, J. Woo, E. Cha, S. Lee, K. Moon, J. Song, Y. Koo and H. Hwang, *Adv. Mater.*, 2015, **27**, 59.
24 Y. C. Yang, F. Pan, Q. Liu, M. Liu and F. Zeng, *Nano Lett.*, 2009, **9**, 1636.
25 Y. Yang and W. Lu, *Nanoscale*, 2013, **5**, 10076.
26 W. A. Hubbard, A. Kerelsky, G. Jasmin, E. R. White, J. Lodico, M. Mecklenburg and B. C. Regan, *Nano Lett.*, 2015, **15**, 3983.
27 N. Onofrio, D. Guzman and A. Strachan, *Nat. Mater.*, 2015, **14**, 440.
28 D. Panda and T.-Y. Tseng, *Ferroelectrics*, 2013, **471**, 23.
29 A. Asamitsu, Y. Tomioka, H. Kuwahara and Y. Tokura, *Nature*, 1997, **388**, 50.
30 Y. Tomioka, A. Asamitsu, H. Kuwahara, Y. Moritomo and Y. Tokura, *Phys. Rev. B*, 1996, **53**, R1689.
31 D.-J. Seong, M. Hassan, H. Choi, J. Lee, J. Yoon, J.-B. Park, W. Lee, M.-S. Oh and H. Hwang, *IEEE Electron Device Lett.*, 2009, **30**, 919.
32 Z. Liao, P. Gao, Y. Meng, H. Zhao, X. Bai, J. Zhang and D. Chen, *Appl. Phys. Lett.*, 2011, **99**, 113506.
33 J. Norpoth, S. Mildner, M. Scherff, J. Hoffmann and C. Jooss, *Nanoscale*, 2014, **6**, 9852.
34 A. Herpers, C. Lenser, C. Park, F. Offi, F. Borgatti, G. Panaccione, S. Menzel, R. Waser and R. Dittmann, *Adv. Mater.*, 2014, **26**, 2730.
35 M. Scherff, B. Meyer, J. Hoffmann, C. Jooss, M. Feuchter and M. Kamlah, *New Journal of Physics*, 2015, **17**, 033011.
36 H.-S. Lee, H.-H. Park and M. J. Rozenbeerg, *Nanoscale*, 2015, **7**, 6444.
37 H. L. Ju, C. Kwon, Q. Li, R. L. Greene and T. Venkatesan, *Appl. Phys. Lett.*, 1994, **65**, 2108.
38 H. Fujishiro, T. Fukase and M. Ikebe, *J. Phys. Soc. Jpn.*, 2001, **70**, 628.
39 G. L. Liu, J. S. Zhou and J. B. Goodenough, *Phys. Rev. B*, 2004, **70**, 224421.
40 C. Moreno, C. Munuera, S. Valencia, F. Kronast, X. Obradors and C. Ocal, *Nano Lett.*, 2010, **10**, 3828.
41 M. Al Ahmad, R. Plana, C. I. Cheon and E. J. Yun, *IEEE Trans. Electron Devices*, 2009, **56**, 665.
42 S. G. Choi, H. S. Lee, H. Choi, S. W. Chung and H. H. Park, *J. Phys. D: Appl. Phys.*, 2011, **44**, 422001.
43 Y. W. Xie, J. R. Sun, D. J. Wang, S. Liang and B. G. Shen, *J. Appl. Phys.*, 2006, **100**, 033704.
44 S. G. Choi, H. S. Lee, H. Choi, S. W. Chung and H. H. Park, *Thin Solid Films*, 2013, **529**, 352.
45 Y. Q. Xiong, W. P. Zhou, Q. Li, Q. Q. Cao, T. Tang, D. H. Wang and Y. W. Du, *Sci. Rep.*, 2015, **5**, 12766.
46 R. Yang, X. M. Li, W. D. Yu, X. D. Gao, D. S. Shang, X. J. Liu, X. Cao, Q. Wang and L. D. Chen, *Appl. Phys. Lett.*, 2009, **95**, 072105.
47 M. Hasan, R. Dong, H. J. Choi, D. S. Lee, D. J. Seong, M. B. Pyun and H. Hwang, *Appl. Phys. Lett.*, 2008, **92**, 202102.
48 Y. Lei and G. Wang, *Scr. Mater.*, 2015, **101**, 20.
49 M. Y. Yang, K. Kamiya, B. Magyari-Kope, M. Niwa, Y. Nishi and K. Shiraishi, *Appl. Phys. Lett.*, 2013, **103**, 093504.
50 K. Kamiya, M. Y. Yang, S.-G. Park, B. Magyari-Kope, Y. Nishi, M. Niwa and K. Shiraishi, *Appl. Phys. Lett.*, 2012, **100**, 073502.
51 B. Magyari-Köpe, S. G. Park, H.-D. Lee and Y. Nishi, *J. Mater. Sci.*, 2012, **47**, 7498.
52 B. Magyari-Köpe, S.-G. Park, H. D. Lee and Y. Nishi, *ECS Trans.*, 2011, **37**, 167.
53 S. H. Jeon, W.-J. Son, B. H. Park and S. Han, *Appl. Phys. A*, 2011, **102**, 909.
54 C. A. F. Vaz, F. J. Walker, C. H. Ahn and S. Ismail-Beigi, *J. Phys.: Condens. Matter*, 2015, **27**, 123001.
55 Y. Tokura, A. Urushibara, Y. Moritomo, T. Arima, A. Asamitsu, G. Kido and N. Furukawa, *J. Phys. Soc. Jpn.*, 1994, **63**, 3931.
56 A. Urushibara, Y. Moritomo, T. Arima, A. Asamitsu, G. Kido and Y. Tokura, *Phys. Rev. B*, 1995, **51**, 14103.
57 N. Abdelmoula, K. Guidara, A. Cheikh-Rouhou, E. Dhahri and J. C. Joubert, *J. Solid State Chem.*, 2000, **151**, 139.
58 Y. M. Baïkov, E. I. Nikulin, B. T. Melekh and V. M. Egorov, *Phys. Solid State*, 2004, **46**, 2086.
59 J. Sakai, N. Ito and S. Imai, *J. Appl. Phys.*, 2006, **99**, 08Q318.
60 V. N. Varyukhin, Y. V. Medvedev, Y. M. Nikolaenko, A. B. Mukhin, B. V. Belyaev, V. A. Gritskikh, I. V. Zhikharev, S. V. Kara-Murza, N. V. Korchikova and A. A. Tikhii, *Tech. Phys. Lett.*, 2009, **35**, 937.
61 H. L. Ju, J. Gopalakrishnan, J. L. Peng, Q. Li, G. C. Xiong, T. Venkatesan and R. L. Greene, *Phys. Rev. B*, 1995, **51**, 6143.
62 N. Lee, Y. Lansac and Y. H. Jang, *J. Nanosci. Nanotechnol.*, 2011, **11**, 339.
63 Y. H. Jang, F. Gervais and Y. Lansac, *J. Chem. Phys.*, 2009, **131**, 094503.
64 J. P. Perdew, K. Burke and M. Ernzerhof, *Phys. Rev. Lett.*, 1997, **78**, 1396.
65 J. P. Perdew, K. Burke and M. Ernzerhof, *Phys. Rev. Lett.*, 1996, **77**, 3865.
66 G. Kresse and J. Furthmuller, *Comput. Mat. Sci.*, 1996, **6**, 15.
67 G. Kresse and D. Joubert, *Phys. Rev. B*, 1999, **59**, 1758.
68 V. Ferrari, J. M. Pruneda and E. Artacho, *Phys. Status Solidi A*, 2006, **203**, 1437.
69 K. Wang, Y. Ma and K. Betzler, *Phys. Rev. B*, 2007, **76**, 144431.
70 J. M. Pruneda, V. Ferrari, R. Rurali, P. B. Littlewood, N. A. Spaldin and E. Artacho, *Phys. Rev. Lett.*, 2007, **99**, 226101.
71 P. Ravindran, A. Kjekshus, H. Fjellvåg, A. Delin and O. Ericksson, *Phys. Rev. B*, 2002, **65**, 644451.
72 P. E. Blöchl, *Phys. Rev. B*, 1994, **50**, 17953.
73 H. J. Monkhorst and J. D. Pack, *Phys. Rev. B*, 1976, **13**, 5188.
74 K. Momma and F. Izumi, *J. Appl. Crystallogr.*, 2011, **44**, 1272.
75 I. Solovyev, N. Hamada and K. Terakura, *Phys. Rev. B*, 1996, **53**, 7158.
76 S. Satpathy, Z. S. Popović and F. R. Vukajlović, *Phys. Rev. Lett.*, 1996, **76**, 960.
77 S. Picozzi, C. Ma, Z. Yang, R. Bertacco, M. Cantoni, A. Cattoni, D. Petti, S. Brivio and F. Ciccacci, *Phys. Rev. B*, 2007, **75**, 094418.

78 D. Petti, A. Stroppa, S. Picozzi, S. Brivio, M. Cantoni and R. Bertacco, *J. Magn. Magn. Mater.*, 2012, **324**, 2659.
79 M. Pavone, A. B. Muñoz-García, A. M. Ritzmann and E. A. Carter, *J. Phys. Chem. C*, 2014, **118**, 13346.
80 A. B. Muñoz-García, A. M. Ritzmann, M. Pavone, J. A. Keith and E. A. Carter, *Acc. Chem. Res.*, 2014, **47**, 3340.
81 A. M. Deml, V. Stevanović, A. M. Holder, M. Sanders, R. O'Hayre and C. B. Musgrav, *Chem. Mater.*, 2014, **26**, 6595.
82 W. Tang, E. Sanville and G. Henkelman, *J. Phys.: Condens. Matter*, 2009, **21**, 084204.
83 E. Sanville, S. D. Kenny, R. Smith and G. Henkelman, *J. Comput. Chem.*, 2007, **28**, 899.
84 G. Henkelman, A. Arnaldsson and H. Jónsson, *Comput. Mater. Sci.*, 2006, **36**, 354.
85 O. Chmaissem, B. Dabrowski, S. Kolesnik, J. Mais, J. D. Jorgensen and S. Short, *Phys. Rev. B*, 2003, **67**, 944311.
86 M. Brandbyge, J.-L. Mozos, P. Ordejón, J. Taylor and K. Stokbro, *Phys. Rev. B*, 2002, **65**.
87 J. M. Soler, E. Artacho, J. D. Gale, A. García, J. Junquera, P. Ordejón and D. Sánchez-Portal, *J. Phys.: Condens. Matter*, 2002, **14**.
88 N. Troullier and J. L. Martins, *Phys. Rev. B*, 1991, **43**, 1993.
89 S. K. Estemirova, A. M. Yankin, S. G. Titova, V. F. Balakirev and Y. E. Turkhan, *Inorg. Mater.*, 2008, **44**, 1251.
90 J. Rodríguez-Carvajal, M. Hennion, F. Moussa, A. H. Moudden, L. Pinsard and A. Revcolevschi, *Phys. Rev. B*, 1998, **57**, R3189.
91 Y. Murakami, J. P. Hill, D. Gibbs, M. Blume, I. Koyama, M. Tanaka, H. Kawata, T. Arima, Y. Tokura, K. Hirota and Y. Endoh, *Phys. Rev. Lett.*, 1998, **81**, 582.
92 J. S. Zhou and J. B. Goodenough, *Phys. Rev. B*, 1999, **60**, R15002.
93 J. B. A. A. Elemans, B. Van Laar, K. R. Van Der Veen and B. O. Loopstra, *J. Solid State Chem.*, 1971, **3**, 238.
94 P. Norby, I. G. K. Andersen, E. K. Andersen and N. H. Andersen, *J. Solid State Chem.*, 1995, **119**, 191.
95 M. N. Iliev, M. V. Abrashev, H. G. Lee, V. N. Popov, Y. Y. Sun, C. Thomsen, R. L. Meng and C. W. Chu, *Phys. Rev. B*, 1998, **57**, 2872.
96 T. Mori, K. Inoue and N. Kamegashira, *J. Alloys Compd.*, 2000, **308**, 87.
97 T. Negas and R. S. Roth, *J. Solid State Chem.*, 1970, **1**, 409.
98 K. Kuroda, N. Ishizawa, N. Mizutani and M. Kato, *J. Solid State Chem.*, 1981, **38**, 297.
99 P. D. Battle, T. C. Gibb and C. W. Jones, *J. Solid State Chem.*, 1988, **74**, 60.
100 A. Daoud-Aladine, C. Martin, L. C. Chapon, M. Hervieu, K. S. Knight, M. Brunelli and P. G. Radaelli, *Phys. Rev. B*, 2007, **75**, 104417.
101 O. Chmaissem, B. Dabrowski, S. Kolesnik, J. Mais, D. E. Brown, R. Kruk, P. Prior, B. Pyles and J. D. Jorgensen, *Phys. Rev. B*, 2001, **64**, 1344121.
102 L. Rørmark, K. Wiik, S. Stølen and T. Grande, *J. Mater. Chem.*, 2002, **12**, 1058.
103 T. Takeda and S. Ohara, *J. Phys. Soc. Jpn.*, 1974, **37**, 275.
104 J. B. Goodenough, *Phys. Rev.*, 1955, **100**, 564.
105 E. O. Wollan and W. C. Koehler, *Phys. Rev.*, 1955, **100**, 545.
106 J. Heyd, G. E. Scuseria and M. Ernzerhof, *J. Chem. Phys.*, 2006, **124**, 219906.
107 A. V. Krukau, O. A. Vydrov, A. F. Izmaylov and G. E. Scuseria, *J. Chem. Phys.*, 2006, **125**, 224106.
108 J. F. Mitchell, D. N. Argyriou, C. D. Potter, D. G. Hinks, J. D. Jorgensen and S. D. Bader, *Phys. Rev. B*, 1996, **54**, 6172.
109 P. Kameli, H. Salamati, A. Heidarian and H. Bahrami, *J. Non-Cryst. Solids*, 2009, **355**, 917.
110 S. V. Trukhanov, I. O. Troyanchuk, I. A. Bobrikov, V. G. Simkin and A. M. Balagurov, *Crystallogr. Rep.*, 2007, **52**, 805.
111 P. M. Woodward, T. Vogt, D. E. Cox, A. Arulraj, C. N. R. Rao, P. Karen and A. K. Cheetham, *Chem. Mater.*, 1998, **10**, 3652.
112 J. Hemberger, A. Krimmel, T. Kurz, H. A. Krug von Nidda, V. Y. Ivanov, A. A. Mukhin, A. M. Balbashov and A. Loidl, *Phys. Rev. B*, 2002, **66**, 944101.
113 B. Zheng and N. Binggeli, *J. Phys.: Condens. Matter*, 2009, **21**, 115602.
114 T. Geng and N. Zhang, *Phys. Lett. A*, 2006, **351**, 314.
115 G. Banach and W. M. Temmerman, *Phys. Rev. B*, 2004, **69**, 544271.
116 A. Asamitsu and Y. Tokura, *Phys. Rev. B*, 1998, **58**, 47.
117 K. Horiba, A. Chikamatsu, H. Kumigashira, M. Oshima, N. Nakagawa, M. Lippmaa, K. Ono, M. Kawasaki and H. Koinuma, *Phys. Rev. B*, 2005, **71**, 155420.
118 W. L. Huang, Q. Zhu, W. Ge and H. Li, *Comput. Mater. Sci.*, 2011, **50**, 1800.
119 J. Nowotny and M. Rekas, *J. Am. Ceram. Soc.*, 1998, **81**, 67.
120 Y. Choi, D. S. Mebane, M. C. Lin and M. Liu, *Chem. Mater.*, 2007, **19**, 1690.
121 G. Henkelman, B. P. Uberuaga and H. Jónsson, *J. Chem. Phys.*, 2000, **113**, 9901.
122 G. Henkelman and H. Jónsson, *J. Chem. Phys.*, 2000, **113**, 9978.
123 M. Cherry, M. S. Islam and C. R. A. Catlow, *J. Solid State Chem.*, 1995, **118**, 125.
124 M. S. Islam, *J. Mater. Chem.*, 2000, **10**, 1027.
125 M. S. Islam, *Solid State Ionics*, 2002, **154-155**, 75.
126 S. M. Woodley, J. D. Gale, P. D. Battle, C. Richard and A. Catlow, *J. Chem. Phys.*, 2003, **119**, 9737.
127 A. Belzner, T. M. Gür and R. A. Huggins, *Solid State Ionics*, 1992, **57**, 327.
128 B. Nadgorny, I. I. Mazin, M. Osofsky, Soulen R.J, Jr., P. Broussard, R. M. Stroud, D. J. Singh, V. G. Harris, A. Arsenov and Y. Mukovskii, *Phys. Rev. B*, 2001, **63**, 1844331.
129 M. Yoshimoto, H. Maruta, T. Ohnishi, K. Sasaki and H. Koinuma, *Appl. Phys. Lett.*, 1998, **73**, 187.